Research Paper

Brain and Neuroscience Advances

Brain and Neuroscience Advances
Volume 6: 1–13

DOI: 10.1177/23982128221086464
journals.sagepub.com/home/bna
SAGE

Reducing voltage-dependent potassium channel Kv3.4 levels ameliorates synapse loss in a mouse model of Alzheimer's disease

Jie Yeap[1], Chaitra Sathyaprakash[1], Jamie Toombs[1], Jane Tulloch[1], Cristina Scutariu[1], Jamie Rose[1], Karen Burr[2], Caitlin Davies[1], Marti Colom-Cadena[1], Siddharthan Chandran[2], Charles H. Large[3], Matthew J. M. Rowan[4], Martin J. Gunthorpe[3] and Tara L. Spires-Jones[1]

Abstract

Synapse loss is associated with cognitive decline in Alzheimer's disease, and owing to their plastic nature, synapses are an ideal target for therapeutic intervention. Oligomeric amyloid beta around amyloid plaques is known to contribute to synapse loss in mouse models and is associated with synapse loss in human Alzheimer's disease brain tissue, but the mechanisms leading from Aβ to synapse loss remain unclear. Recent data suggest that the fast-activating and -inactivating voltage-gated potassium channel subtype 3.4 (Kv3.4) may play a role in Aβ-mediated neurotoxicity. Here, we tested whether this channel could also be involved in Aβ synaptotoxicity. Using adeno-associated virus and clustered regularly interspaced short palindromic repeats technology, we reduced Kv3.4 expression in neurons of the somatosensory cortex of APP/PS1 mice. These mice express human familial Alzheimer's disease-associated mutations in amyloid precursor protein and presenilin-1 and develop amyloid plaques and plaque-associated synapse loss similar to that observed in Alzheimer's disease brain. We observe that reducing Kv3.4 levels ameliorates dendritic spine loss and changes spine morphology compared to control virus. In support of translational relevance, Kv3.4 protein was observed in human Alzheimer's disease and control brain and is associated with synapses in human induced pluripotent stem cell–derived cortical neurons. We also noted morphological changes in induced pluripotent stem cell neurones challenged with human Alzheimer's disease-derived brain homogenate containing Aβ but, in this in vitro model, total mRNA levels of Kv3.4 were found to be reduced, perhaps as an early compensatory mechanism for Aβ-induced damage. Overall, our results suggest that approaches to reduce Kv3.4 expression and/or function in the Alzheimer's disease brain could be protective against Aβ-induced synaptic alterations.

Keywords

Voltage-gated potassium channel, Alzheimer, synapse

Received: 24 November 2021; accepted: 18 February 2022

Introduction

Alzheimer's disease (AD) is characterised by the progressive accumulation of amyloid plaques and neurofibrillary tangles, composed of abnormally aggregated β-amyloid (Aβ) and hyperphosphorylated tau proteins, respectively (Serrano-Pozo et al., 2011). Along with these neuropathological lesions, there is extensive neuronal loss, synapse loss and gliosis (Henstridge et al., 2019). Of these brain changes, synapse loss is the strongest correlate of cognitive decline in AD (DeKosky and Scheff, 1990; Terry et al., 1991), and synapses, with their myriad receptors and ion channels, are attractive therapeutic targets for intervention (Colom-Cadena et al., 2020). In brains affected by AD and in mouse models of amyloid plaque formation, plaques act as a local reservoir of oligomeric Aβ,

[1]UK Dementia Research Institute and Centre for Discovery Brain Sciences, The University of Edinburgh, Edinburgh, UK
[2]UK Dementia Research Institute and Centre for Clinical Brain Sciences, The University of Edinburgh, Edinburgh, UK
[3]Autifony Therapeutics Limited, Stevenage Bioscience Catalyst, Stevenage, UK
[4]Emory University School of Medicine, Atlanta, GA, USA

Corresponding author:
Tara L. Spires-Jones, UK Dementia Research Institute and Centre for Discovery Brain Sciences, The University of Edinburgh, 1 George Square, Edinburgh EH8 9JZ, UK.
Email: Tara.spires-jones@ed.ac.uk

emanating these soluble and diffusible Aβ species to form a halo surrounding plaques which is associated with synapse loss (Koffie et al., 2009, 2012; Spires-Jones and Hyman, 2014). While the synaptotoxicity of oligomeric Aβ is well-established, it is not yet entirely clear how synapses are damaged or whether this can be recovered by therapeutic interventions.

One potential pathway mediating Aβ synaptotoxicity involves voltage-gated potassium channels. The voltage-gated potassium channel subtype 3.4 (Kv3.4) encoded by the *KCNC4* gene is a member of the Kv3 family of channels that play important roles in controlling neuronal firing and contribute to synaptic plasticity (Kaczmarek and Zhang, 2017; Rowan and Christie, 2017). This channel is believed to have vital roles in regulating neurotransmitter release and mediating neuronal excitability and plasticity given its pre- and post-synaptic localisation (Kaczmarek and Zhang, 2017; Rowan et al., 2016). Dysregulation of Kv3.4 channel expression has been implicated in several neurological conditions due to its role in pathways linked to oxidative stress and hypoxia (Kypo et al., 2005; Song et al., 2017). Kv3 channels are also involved in signalling pathways linked to neurodegenerative diseases such as spinal cerebellar ataxia (Zhang and Kaczmarek, 2016). In early and late stages of AD, Kv3.4 gene expression was increased in a study of frontal cortex from seven donors (two control, three early AD and two late AD cases) (Angulo et al., 2004). In this same study, protein level measured by western blot was also increased in AD compared to control frontal cortex, and Kv3.4 staining with immunohistochemistry was observed in a punctate pattern in all cases, with some accumulation around plaques in AD samples (Angulo et al., 2004). Furthermore, increased Kv3.4 protein levels were observed in three Tg2576 transgenic mice (which develop amyloid plaques) compared to three wild-type (WT) mice (Angulo et al., 2004). A subsequent study in the same mouse line specifically demonstrated astrocytic upregulation of Kv3.4 and that lowering Kv3.4 levels caused downregulation of a reactive astrocyte marker and Aβ oligomers (Boscia et al., 2017). This observation may be linked with the notion that the Kv3.4-mediated K^+ efflux is implicated in the activation of astrocytic inflammasomes and reduced astrocytic phagocytosis in the early stages of AD (Boscia et al., 2017; Piccialli et al., 2020). High concentrations of Aβ (5 μM) applied to rat primary hippocampal neuronal cultures or differentiated PC12 cells also induced Kv3.4 expression and morphological abnormalities which could be prevented by inhibiting Kv3.4 channel activity (Ciccone et al., 2019; Pannaccione et al., 2007).

Here, we tested the hypothesis that Kv3.4 channels play an important role in pathways that mediate toxicity towards synapses in the Alzheimer's brain and that reducing levels of this channel can protect synapses from Aβ-induced degeneration. To test this hypothesis, we examined dendritic spines in plaque-bearing APP/PS1 mice and littermate controls with and without lowering Kv3.4 expression. Further, we examine human-induced pluripotent stem cell (iPSC)-derived cortical neurons and human post-mortem brain tissue to determine whether Kv3.4 is indeed expressed in synapses where it may mediate Aβ toxicity.

Materials and methods

Mice

APPswe/PS1dE9 (APP/PS1, n = 10) mice originally purchased from Jackson Laboratory (Bar Harbor, ME, USA) were bred and aged in house. These double transgenic mice overexpress a human mutant amyloid precursor protein gene with the Swedish mutation and a human mutant presenilin-1 gene with the deletion of exon 9 (Jankowsky et al., 2004). WT (n = 6) littermates were used as controls. Both sexes of mice were used. All mice were group housed in a 12-h day/night cycle with ad libitum access to food and water. All mice underwent surgery for stereotaxic injections at 7 months of age and were sacrificed 7 weeks post-injection for brain collections. Table 1 shows a summary of the mice used in this study. Experiments were performed in accordance with the UK Animal (Scientific Procedures) Act 1986 and the Directive 2010/63EU of the European Parliament and the Council on the protection of animals used for scientific purposes.

Viral vectors

Adeno-associated viruses (AAVs) were used encoding the red fluorescent protein tdTomato, enhanced yellow fluorescent protein (eYFP) or the single guide RNA (sgRNA) that cleaves *Kv3.4/KCNC4*: pENN.AAV.CAG.tdTomato.WPRE.SV40 (Addgene #105554), pAAV.CamKII(1.3).eYFP.WPRE.hGH (Addgene #10522), U6.sgRNA(mKv3.4).CMV.saCas9, respectively. Prior to use, 2 μL of pENN.AAV.CAG.tdTomato.WPRE.SV40 (1×10^{13} GC/mL) was diluted with an equal volume of 0.1 M phosphate buffer saline (PBS) while 2 μL of pAAV.CamKII(1.3).eYFP.WPRE.hGH (1×10^{13} GC/mL) was mixed with 2 μL of U6.sgRNA(mKv3.4).CMV.saCas9 (1×10^{11} GC/mL).

Stereotaxic surgery

At 7 months of age, mice were anaesthetised with isoflurane (3% for induction, 0.5%–2% for maintenance). Fur on the head of the mice was shaved and Viscotears liquid gel was applied over both eyes before the animals were secured using ear bars in a stereotaxic apparatus. Body temperature was regulated using a heating pad and a rectal probe thermometer. After sterilising the surgical site with betadine and isopropyl alcohol, and performing local anaesthesia with subcutaneous injection of xylocaine (2 μg/g body weight), a 2–3 mm incision was made in the scalp to expose the skull. Burr holes were drilled in the skull, 1.5 mm bilaterally and 1 mm posterior to bregma. Using a 10-μL Hamilton syringe, 4 μL of viral preparation was injected 0.7 mm deep into each burr hole on both somatosensory cortices at a rate of 420 nL/s. Each hemisphere was randomly assigned to either experimental (Kv3.4-knockdown) or control condition and received corresponding AAV viral injections into the somatosensory cortex (Kv3.4-knockdown hemisphere: pAAV.CamKII(1.3).eYFP.WPRE.hGH: U6.sgRNA(mKv3.4).CMV.saCas9, 1:1; control hemisphere: pENN.AAV.CAG.tdTomato.WPRE.SV40: PBS, 1:1). After injections, the scalp was sutured and mice were allowed to recover from anaesthesia in a heated chamber. Injected mice were singly housed under standard conditions until brains were harvested.

Mouse brain tissue processing

After a 7-week incubation period to allow viral expression in neurons, the mice were euthanised and perfused transcardially with PBS followed by 4% paraformaldehyde (PFA; Agar Scientific, Stansted, UK AGR1026). The brains extracted from

Table 1. Summary of mice used in this study. Only a subset of APP/PS1 mice were analysed for Kv3.4 staining intensity.

Mouse ID	Genotype	Sex	Spine density, *Mean (N dendritic segments)*				Kv3.4 intensity (normalised to background), *Mean (N cell bodies)*	
			tdTomato (control)		eYFP (Kv3.4 knockdown)		tdTomato (control)	eYFP (Kv3.4 knockdown)
			Far	Near	Far	Near		
TS23	WT	F	1.82 (20)	N.A.	2.38 (20)	N.A.	3.10 (14)	2.34 (10)
TS25	WT	F	2.11 (20)	N.A.	2.52 (20)	N.A.	2.65 (10)	2.32 (10)
TS511	WT	M	1.59 (20)	N.A.	2.37 (20)	N.A.	2.79 (13)	2.34 (16)
TS517	WT	F	1.77 (20)	N.A.	2.42 (20)	N.A.	2.30 (9)	2.30 (11)
TS531	WT	M	2.07 (20)	N.A.	2.12 (20)	N.A.	2.46 (10)	2.00 (14)
TS532	WT	M	0.80 (20)	N.A.	1.17 (20)	N.A.	1.85 (11)	1.48 (10)
TS476	APP/PS1	F	0.66 (20)	0.58 (24)	0.64 (20)	0.48 (32)	–	–
TS478	APP/PS1	F	0.72 (10)	0.53 (37)	0.66 (19)	0.52 (30)	–	–
TS481	APP/PS1	M	0.80 (12)	0.61 (26)	1.33 (23)	0.79 (24)	–	–
TS499	APP/PS1	F	0.48 (26)	0.46 (37)	0.49 (12)	0.46 (29)	–	–
TS518	APP/PS1	F	0.44 (13)	0.48 (10)	0.68 (39)	0.85 (38)	–	–
TS520	APP/PS1	M	1.43 (20)	0.73 (20)	1.20 (20)	0.88 (20)	2.40 (10)	1.98 (14)
TS526	APP/PS1	F	0.83 (20)	0.50 (20)	1.59 (20)	1.17 (20)	3.20 (10)	2.43 (11)
TS533	APP/PS1	F	2.04 (20)	1.33 (20)	2.26 (18)	1.92 (23)	3.22 (10)	2.36 (11)
TS538	APP/PS1	M	1.39 (20)	0.57 (20)	1.78 (20)	1.37 (20)	2.36 (11)	2.17 (11)
TS546	APP/PS1	M	1.45 (20)	0.75 (18)	1.72 (20)	1.06 (20)	4.81 (12)	2.04 (12)

Kv3.4: voltage-gated potassium channel subtype 3.4; eYFP: enhanced yellow fluorescent protein; WT: wild-type; N.A.: not applicable.

the skull and post-fixed at 4 °C for 2 h before they were sectioned on a vibratome. Coronal sections of 50 µm thickness were collected between bregma 0 and −2 to include the injection sites within the somatosensory cortices. Brain slices with eYFP (visualisation of Kv3.4-knockdown condition) and tdTomato (control condition) expression were isolated after a quick examination under an epifluorescence microscope. These eYFP- and tdTomato-positive slices were then post-fixed in 4% PFA for another 20 min and stored in PBS at 4 °C until use.

Immunohistochemistry and microscopy

For measurement of Kv3.4 expression within injection sites, 50 µm floating slices were stained with an antibody specific to Kv3.4 (Alomone Labs, APC-019) and an anti-rabbit Alexa Fluor Plus 647-conjugated secondary antibody (Invitrogen, Wlatham MA USA, A32795). After blocking the brain slices in 0.5% Triton-X 100 in PBS containing 3% normal donkey serum for an hour, samples were incubated with the primary antibody solution (1:200 dilution in blocking buffer) at 4 °C overnight. The slices were washed in PBS and left in secondary antibody solution (1:5000 dilution in blocking buffer) for 2 h. To stain plaques, brain slices were mounted on microscope slides which were then dipped in 0.05% Thioflavin S in 50% ethanol for 8 min, followed by differentiation with 80% ethanol for 15 s. Immu-mount (Thermo Fisher Scientific (Waltham, MA, USA), #9990402) was applied before the samples were covered with a glass coverslip.

Confocal imaging and analysis of mouse brains

To confirm Kv3.4 reduction in the experimental versus control hemisphere, image stacks (61.5 µm × 61.5 µm × 10–28 µm with a z-step 0.3 µm, 63× zoom 3, N.A. 1.4) of tdTomato- and eYFP-positive cell bodies (n = ∼10 images per mouse) were acquired on a Leica TCS SP8 confocal microscope using laser excitation at 488 nm for eYFP, 552 nm for tdTomato and 638 nm for Kv3.4 staining with Alexa Fluor Plus 647-conjugated secondary. Using ImageJ (Schneider et al., 2012), the mean intensity of Kv3.4 staining of cell bodies was measured. The Kv3.4 staining intensities of cell bodies were normalised to background intensity measured in the same stack and z-section. Table 1 summarises the number of cell bodies analysed and the mean staining intensity of each animal. Mice were excluded from the study only if there was no viral expression detectable by YFP or tdTomato.

To examine the effect of Kv3.4-knockdown on dendritic spine densities, image stacks (61.5 µm × 61.5 µm × 3–25 µm with a z-step 0.3 µm, 63× zoom 3, N.A. 1.4) of dendritic segments, either labelled with eYFP or tdTomato, from cortical layer II, III and V pyramidal neurons were acquired. Only dendritic segments more than 20 µm in length were selected. For every APP/PS1 mouse, dendritic segments were captured for each condition: eYFP-positive, near a plaque (0–30 µm, using laser excitation 405 nm for ThioS staining); eYFP-positive, far from plaques (>30 µm); tdTomato-positive, near a plaque and tdTomato-positive, far from plaques. As WT mice do not present plaques, dendrite selection was made without regard to plaque proximity. Prior to image analysis, all images were randomly code-blinded by an observer and the quantification of spine densities was performed on greyscale images, thereby avoiding experimenter bias. Z-stack reconstructions and measurements were performed in ImageJ. The distance of dendrite segments to the nearest plaque, if present, was measured. The selected dendritic segments were traced in details to count the number of spines present and their morphological class recorded, either as mushroom, thin, stubby or branched. Branched spines had more than one head (Harris et al., 1992; Peters & Kaiserman-Abramof, 1970; Spires, 2005).

Mushroom spines had a clear protrusion with head diameter ⩾2× neck diameter. Thin spines had similar head and neck diameter (head diameter < 2× neck diameter), while stubby spines had no visible neck (head diameter < neck diameter). The length of dendrite segments was measured to calculate linear spine density (n spine per μm along the dendrite). Dendritic shaft diameters were also measured at each end and the midpoint of each segment to produce an average diameter. The number of dendritic segments analysed and the mean spine density of each animal are shown in Table 1.

Human subjects

The use of human tissue for post-mortem studies has been reviewed and approved by the Edinburgh Brain Bank ethics committee and the ACCORD medical research ethics committee, AMREC (ACCORD is the Academic and Clinical Central Office for Research and Development, a joint office of the University of Edinburgh and NHS Lothian, approval no. 15-HV-016). The Edinburgh Brain Bank is a Medical Research Council funded facility with research ethics committee (REC) approval (11/ES/0022). The use of human stem cell derived neurons was approved by the NHS Lothian REC (10/S1103/10).

Western blots of human brain tissue

The concentrations of protein samples from human brain whole homogenate preparations were measured via the bicinchoninic acid (BCA) assay (micro BCA protein assay kit, Thermo Fisher Scientific). 20 μg of total protein were mixed 1:1 with Laemmli buffer and boiled at 95 °C for 10 min, and loaded to NuPAGE™ 4%–12%, Bis-Tris gels. Gels were run at 120 V, 400 mA, >2 h, until the loading dye ran to the bottom of the gel. A protein molecular ladder (Colour Prestained Protein Standard, Broad Range 11–245 kDa, NEB, P7712S) was used as a standard to determine molecular weights. Dry transfer was performed using an iBlot™ 2 gel transfer device (Invitrogen) (8.5 min, 20 V) onto a polyvinylidene difluoride (PVDF) membrane. Membranes were briefly washed in PBS and then immersed in Revert™ 700 Total Protein Stain for 5 min at room temperature. Membranes were immediately washed in Revert 700 Wash Solution, exposed at 700 nm for 1 min and imaged (Odyssey® Fc, LI-COR, Lincoln, NE, USA). Membranes were washed (Revert Destaining Solution) and blocked for 1 h at room temperature (LI-COR Blocking buffer mixed 1:1 with PBS enriched with 0.1% Tween-20 in PBS-T). Membranes were incubated with primary antibody (anti-KCNC4; Alomone Labs, Jerusalem Israel, #APC-019; 1:200) overnight at 4 °C in blocking buffer. Following 3× 10 min washes in PBS-T, membranes were incubated with horseradish peroxidase-conjugated (HRP) secondary antibodies (goat anti-rabbit-HRP; 1:5000) in blocking buffer for 1 h, at room temperature. Membranes were washed 3× 30 min in PBS-T followed by incubation with Amersham™ ECL™ Prime Western Blotting Detection Reagent (Cytiva, Marlborough, MA, USA) to visualise bands. Chemiluminescent bands were visualised using the LI-COR Odyssey® Fc system. Tissue from nine donors was used for this study and their details are found in Supplementary Table 1.

Human iPSC-derived cortical neuron culture

We differentiated five iPSC lines from blood samples of healthy aged people participating in the Lothian Birth Cohort 1936 (LBC1936) study (Toombs et al., 2020). Briefly, peripheral blood mononuclear cells (PBMCs) were reprogrammed using non-integrating oriP/EBNA1 backbone plasmids expressing six iPSC reprogramming factors (OCT3/4 (POU5F1), SOX2, KLF4, L-Myc, shp53, Lin28 and SV40LT). All lines demonstrated Short Tandem Repeat (STR)-matched karyotype. Pluripotency was validated by immunocytochemistry, alkaline phosphatase staining and Pluritest. Tri-lineage differentiation potential was confirmed by hPSC Scorecard and embryoid body formation techniques. All lines were confirmed to be mycoplasma negative. Tissue culture is conducted at 37 °C, 5% CO_2. iPSCs are maintained in six-well culture plates coated with 1:100 Geltrex and fed daily with Essential 8 (E8) media. iPSCs were passaged with 0.1% EDTA pooled at a ratio of 5:1 in six-well culture plates coated with 1:100 Geltrex and fed with E8 media. Differentiation into glutamatergic neurons was conducted by dual SMAD inhibition as described by Shi et al. (2012).

Generation of soluble human brain fraction was conducted according to a published protocol (W. Hong et al., 2018). Brain tissue was chopped and incubated for 30 min in artificial cerebrospinal fluid (CSF) (pH 7.4) supplemented with 1× cOmplete mini EDTA-free protease inhibitor cocktail tablet (Roche (Basel, Switzerland), 11836170001). The tissue/CSF mix was centrifuged at 2000 RCF for 10 min to remove large, insoluble debris then centrifuged at 200,000 RCF for 110 min. The resulting supernatant was dialysed to remove salts and any drugs taken by the donor. The resulting homogenate was immunodepleted to remove soluble amyloid beta or mock immunodepleted using protein A agarose beads (Thermo, 20334) with 4G8 antibody (BioLegend (San Diego, CA, USA), 800703) or mouse serum (Merck, M5905) as a mock condition (W. Hong et al., 2018). Concentration of Aβ1–42 in Aβ+ and Aβ− homogenate was quantified by sandwich enzyme-linked immunoassay (ELISA) (FUJIFILM WAKO, Neuss Germany, 296-64401), according to the manufacturer instructions. For experiments, Aβ+ homogenate was used at a final concentration of 15 pmol/L. Aβ− homogenate approximated the ELISA lower limit of quantification; therefore, Aβ content could not be accurately determined. Aβ− homogenate was diluted by the same factor as Aβ+, with a final concentration considered to be <1 pmol/L.

iPSC-derived cortical neurons were fixed with 4% formalin (Polysciences, cat.04018-1) for 15 min, rinsed in Dulbecco's phosphate buffered saline (D-PBS, Thermo, 14190250) and stored in D-PBS at 4 °C for up to a month before staining. To stain, coverslips containing fixed neurons were permeabilised and non-specific antigens blocked by incubating in D-PBS with 0.2% Triton-X (Merck (Darmstadt, Germany), cat. X100-500ML) and 10% donkey serum (Merck, cat. 566380-10ML) for 1 h. Coverslips were incubated overnight at 4 °C with primary antibodies: Homer (rabbit anti-Homer; Abcam (Cambridge, UK); 1:500), MAP2 (guinea pig anti-MAP2; Synaptic Systems (Göttingen, Germany) 188004; 1:1000), Kv3.4A (sheep anti-Kv3.4A; Autifony (Stevenage, UK) Ab101; 1:100) diluted in D-PBS containing 0.2%

Triton-X and 1% donkey serum. Cells were then washed with D-PBS containing 0.1% Triton-X, and incubated in secondary antibodies diluted 1:500 in D-PBS containing 0.1% Triton-X and 1% donkey serum for 1 h (donkey anti-rabbit-488 (Abcam ab150073), donkey anti-guinea pig-594 (Merck (Darmstadt, Germany), SAB4600096) and donkey anti-sheep-647 (Thermo A21448)). Coverslips were mounted on slides (VWR, 631-0847) with mounting media (Merck, cat. 345789-20ML) and imaged on a Leica TCS confocal microscope with an oil immersion 63× objective. Ten fields per coverslip containing MAP2 staining were randomly selected for imaging and image stacks acquired through the thickness of the cell layer (0.3 µm per step). Image stacks were processed using custom software to segment staining, calculate the density of synaptic markers along MAP2 positive processes, colocalisation of Kv3.4 with Homer 1 post-synaptic terminals, and measure the intensity of Kv3.4 staining in dendrites. All image analysis scripts are freely available at https://github.com/Spires-Jones-Lab.

Aged neurons were incubated with Trizol (Thermo, 15596026) for 5 min. Neurons were homogenised with a P200 pipette and collected in DNase/RNase free tubes (Eppendorf, Hamburg, Germany, 30108051). 200 µL of chloroform (Sigma, St Lois Missouri USA, 288306-100ML) was added per 1 mL Trizol sample and mixed by inversion. Samples were centrifuged at 12,000 RCF for 15 min at 4 °C. The aqueous phase containing RNA was collected and an equal volume of 100% isopropanol added. The sample was centrifuged at 12,000 RCF for 10 min at 4 °C and the supernatant discarded. The pellet was washed in two cycles of 0.5 mL of 70% ethanol and centrifugation at 12,000 RCF for 10 min at 4 °C. The sample was air dried for 10 min at room temperature to evaporate any residual ethanol. The RNA pellet was solubilised in 30 µL DEPC water (Thermo, AM9906) and transferred to a fresh DNase/RNase free Eppendorf, and stored at −80 °C. Concentration and purity were measured using an LVis plate on a ClarioSTAR Plus spectrophotometer (BMG Labtech, Ortenberg, Germany).

Quantitative reverse transcription polymerase chain reaction (RT-qPCR) was conducted using one-step RT-qPCR kit (Promega (Madison, WI, USA), A6020), according to the manufacturer instructions. This product uses advanced BRYT green dye, enabling an RNA detection range of 500 fg and up to 100 ng, and alleviates the need for prior cDNA translation. Briefly, 100 ng RNA samples were added to a master mix preparation (GoTaq qPCR Mastermix (2×), GoScript RT mix for one-step RT-qPCR (50×), Forward Primer (200 nM), Reverse Primer (200 nM) and DEPC H_2O) to a volume of 20 µL per well. Primers are described in Supplementary Table 2. RT-qPCR was conducted in a thermal cycler (Bio-Rad (Hercules, CA, USA), CFX96 Touch Real-Time PCR Detection System), with an initial denaturation step (95 °C, 10 min), then cyclic denaturation (95 °C, 10 s), annealing (60 °C, 30 s) and extension (72 °C, 30 s) for 40 cycles. This was concluded with a melt curve 65–95 °C. Data were analysed with Bio-Rad CFX Maestro software. Target expression was normalised to that of two reference genes (*GAPDH* and *RPLP1*) using the $\Delta\Delta C_q$ method. *GAPDH* and *RPLP1* were determined to be the most stable reference genes of a gene panel tested on iPSC-neurons treated with Aβ+ and Aβ− homogenate, with a NormFinder stability score of 0.09.

Data analysis

Linear mixed effects models were used to analyse data with mouse as a random effect to account for multiple measurements per mouse. Genotype, treatment (Kv3.4 knockdown or control), sex and plaque proximity (in APP/PS1 mice only) were fixed effects in mouse analyses. Assumptions of the model fit were tested by visual inspection of residual plots. Where needed, the data were transformed to better fit model assumptions (transformations noted in results). Analysis of variance tests were run on linear mixed effects models to examine main effects and estimated marginal means with Tukey's corrections were used for post hoc group comparisons. For spine morphology data, Pearson's chi-square tests were used to compare all spines in each treatment group. For correlations with the Plaque distance, repeated measures correlations were conducted for each treatment group separately using a published package (Bakdash and Marusich, 2017). All statistical analyses were run in R Studio and analysis scripts, data files analysed, and analysis outputs including residual plots and Q-Q plots for models are provided as Supplemental Information. Data are presented as box plots of data from all images analysed with individual data points showing a mean for each mouse or human to show biological variability. All data, graphs and statistical analyses included in this article are freely available on the University of Edinburgh Data Share Repository in our laboratories data sharing collection at https://datashare.ed.ac.uk/handle/10283/3076.

Results

To test the hypothesis that Kv3.4 downregulation ameliorates dendritic spine loss associated with amyloid pathology, APP/PS1 mice and WT control mice were injected with an AAV containing the sgRNA targeting *Kv3.4/KCNC4* into neurons of their somatosensory cortex, thereby decreasing Kv3.4 levels in this region. This AAV was co-injected with an AAV that introduced the gene for eYFP which allowed fluorescent visualisation of neurons. The contralateral hemisphere which was injected with an AAV to express the tdTomato reporter in cells served as a within-animal control condition. A total of 10 APP/PS1 mice and 6 WT mice were used in this study. The Kv3.4-knockdown by AAV was assessed by measuring fluorescence intensity of Kv3.4 staining in a subset of the animals used (n = 5 APP/PS1; n = 6 WT mice). To examine synapse loss, dendrites labelled with eYFP/tdTomato were investigated in all mice, near (0–30 µm) and far (>30 µm) from plaques (if present), using confocal microscopy and measurements for dendritic spine density were produced using image stacks.

We observed a 21% decrease in Kv3.4 staining intensity in eYFP-expressing neurons in which Kv3.4 was knocked down compared to tdTomato-expressing control neurons (Figure 1, linear mixed-effects model on Tukey's transformed data followed by analysis of variance (ANOVA), $F[1,39.37] = 38.22$, $p < 0.0001$; no primary negative controls for staining are shown in Supplemental Figure 1). There was no significant effect of sex or genotype, nor was there an interaction between treatment and genotype.

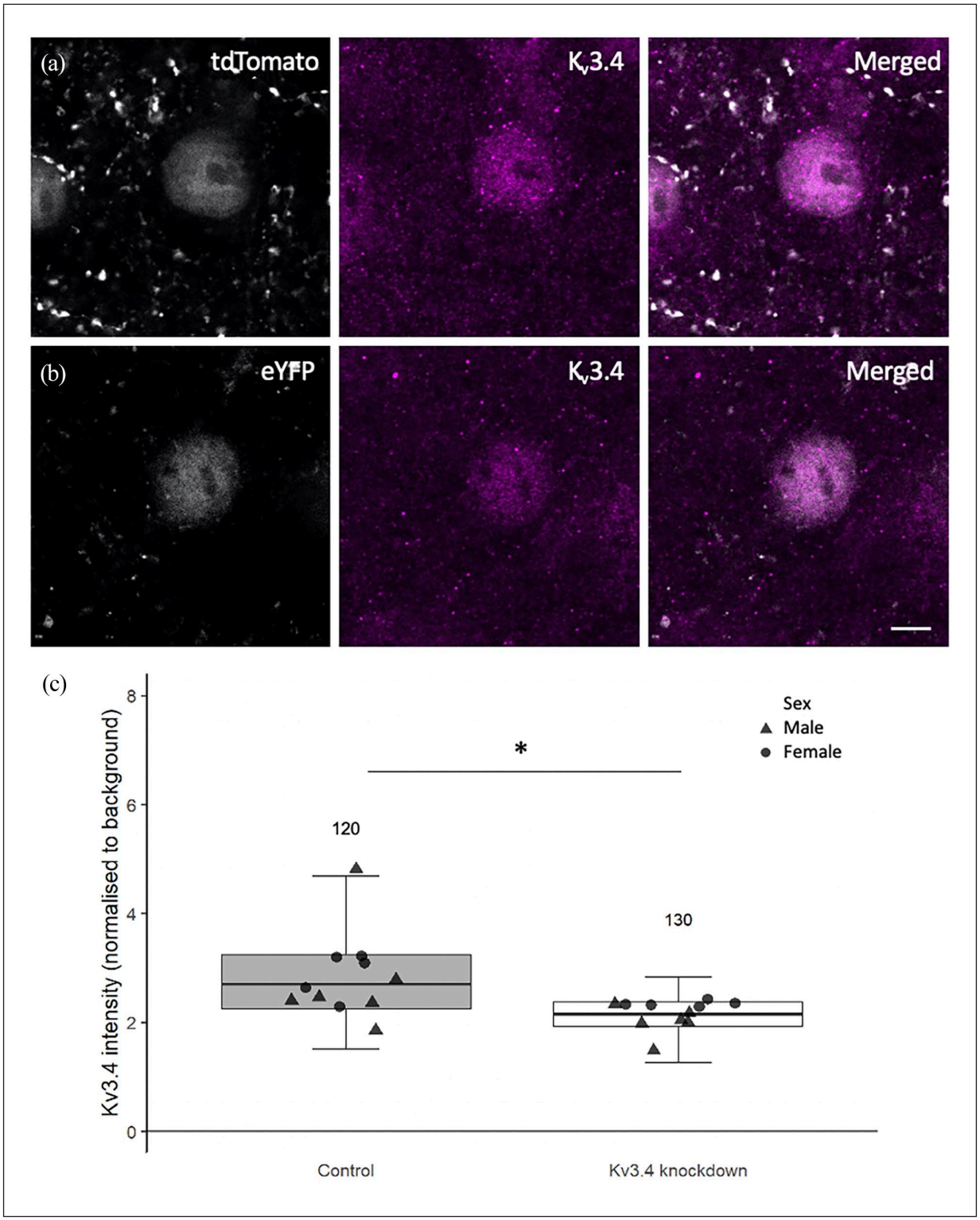

Figure 1. Representative immunostaining images of Kv3.4 in neurons expressing either tdTomato or eYFP (a and b). For comparison purposes, tdTomato and eYFP cell bodies are visualised in grey pseudo-colour and Kv3.4 staining in magenta. Compared to the tdTomato-filled neuron, the eYFP-filled neuron shows lower Kv3.4 immunoreactivity. Analysis of Kv3.4 immunostaining intensity revealed a 21% reduction in staining intensity in eYFP-filled cells relative to tdTomato-filled cells (c), confirming the action of U6.sgRNA(mKv3.4).CMV.saCas9 at knocking down Kv3.4 levels. N above error bars represent the number of cells analysed for each condition. Individual data point shows mean per mouse. Scale bar is 5 μm.
*$p < 0.0001$ ANOVA effect of treatment.

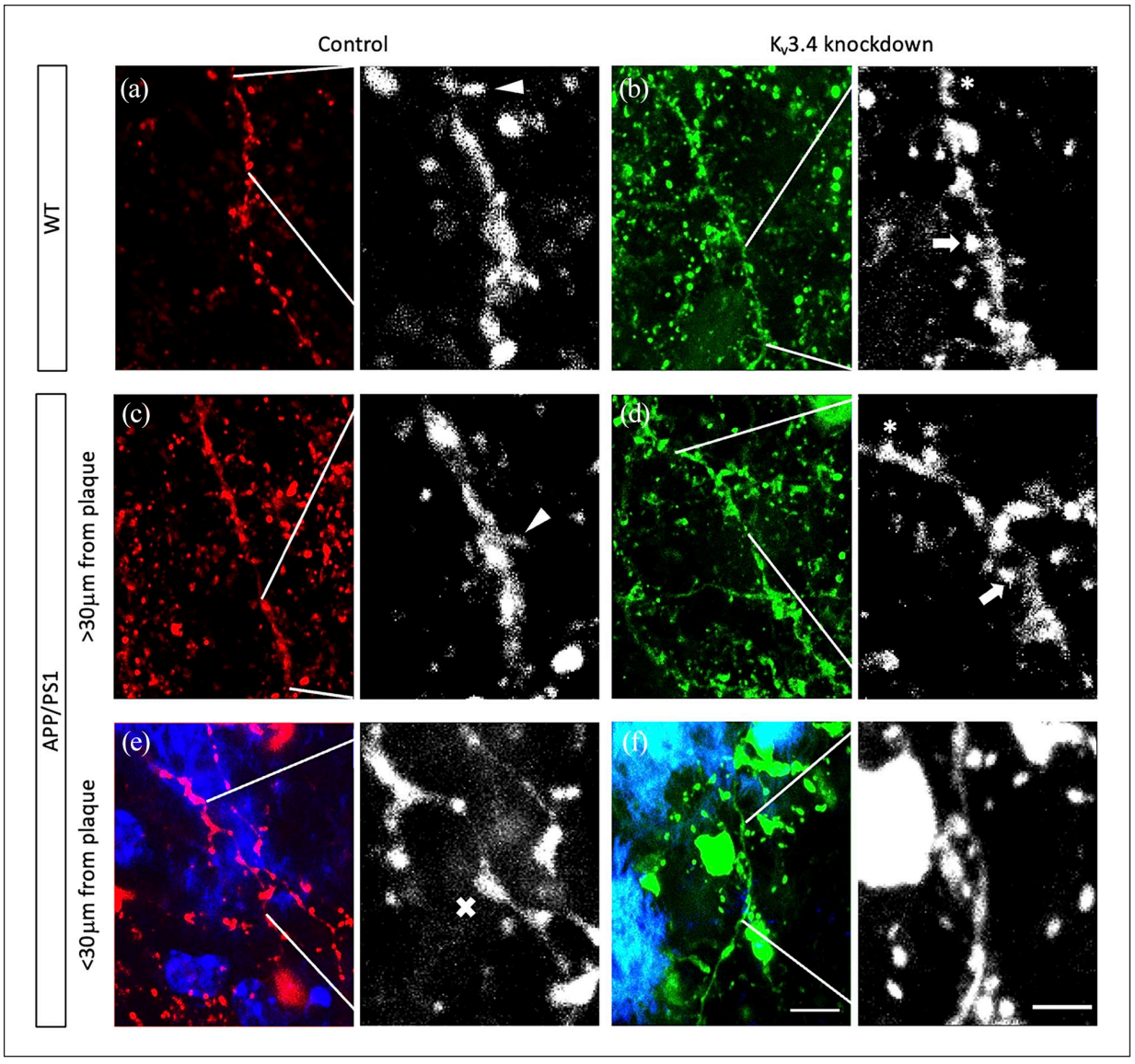

Figure 2. Dendritic spines were examined on dendrites from cortical pyramidal neurons filled with tdTomato or eYFP under control ((a), (c) and (e)) or Kv3.4 knockdown conditions ((b), (d) and (f)), respectively. Spines were classified by shape as either mushroom (arrows), thin (arrowheads) or stubby (asterisks) based on the head to neck diameter ratio. Senile plaques in APP/PS1 mice were labelled in blue using ThioS ((e) and (f)). There is visible focal swelling (crosses) of dendritic segments that are in close proximity to plaques ((e) and (f)). Images are shown as maximum intensity Z-projections of nine serial confocal images. Scale bar is 5 μm (left) and 2 μm (right).

A reduction of dendritic spine density near plaques has been consistently reported in AD mouse models, including APP/PS1 mice used in this study (Koffie et al., 2009; Moolman et al., 2004; Rozkalne et al., 2011). Here, to analyse the effects of Kv3.4 reduction on plaque-associated spine loss, we measured dendritic spine density of dendrite branches from layer II, III and V originating from cortical pyramidal neurons filled with eYFP/tdTomato in APP/PS1 and control mice (Figure 2(a)–(f)). In general, the spine density in APP/PS1 transgenic mice was significantly lower compared to WT mice (Figure 3(a), $F[1,13.06]=16.20$, $p=0.001$). Under control conditions, dendrites in APP/PS1 mice had significantly less spines than those in WT mice ($\beta=0.85$, $t=3.52$, $p=0.012$, post hoc estimated marginal means comparison), which is in accord with previous studies (Koffie et al., 2009; Moolman et al., 2004; Rozkalne et al., 2011). There is further a positive correlation between plaque distance and spine density in the tdTomato-filled control dendrites of APP/PS1 mice (Figure 3(c), repeated measures correlation $r_{rm}=0.14$, degree of freedom (df)$=221$, 95% confidence interval (CI)$=0.014$–0.272, $p=0.03$), which was absent in their eYFP-filled Kv3.4-knockdown dendrites (CI$=-0.031$–0.271, $p=0.14$).

Kv3.4 downregulation evidently increased spine density compared to the control hemisphere in both APP/PS1 and WT mice (Figure 3(a), treatment effect $F[1,1102.12]=163.29$, $p<0.0001$)

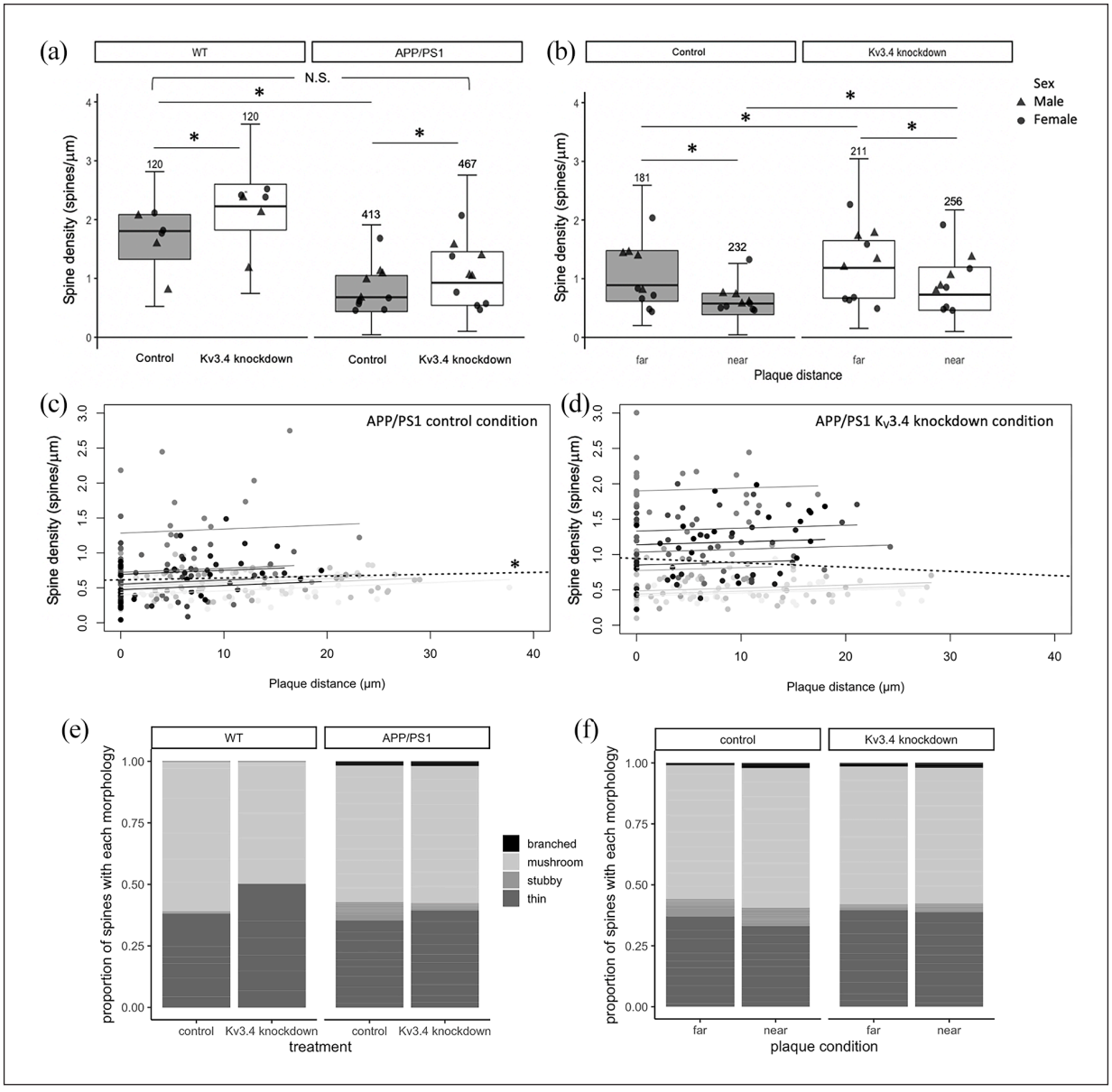

Figure 3. Under control conditions, there is a 62.4% reduction in spine density in APP/PS1 mice compared to WT mice without the APP and PS1 transgenes (a). Kv3.4 knockdown increases spine densities in both wild-type (WT) and APP/PS1 mice relative to control conditions, and restores spine densities in the transgenic mice to near WT control levels. In APP/PS1 mice, lower spine densities were recorded in dendrites within 30 µm of plaques in contrast to those distant from plaques (b). Kv3.4 downregulation improved spine densities in all dendrites measured in APP/PS1 mice ((a) and (b) *$p < 0.05$, post hoc estimated marginal means comparisons with Tukey's correction. N above error bars represent the number of dendrites analysed for each condition. Individual data point shows mean per mouse). Under control conditions, spine density of APP/PS1 mice correlated with distance from the nearest plaque ((c), * $p = 0.03$ repeated measures correlation). This correlation was absent in the Kv3.4 knockdown dendrites, indicating that Kv3.4 knockdown is protective (d). In (c) and (d), data points show individual dendrites shaded to show those from each individual mouse, the regression line for each mouse is shown in the same shade, and the overall regression is the black dotted line. The control hemisphere of APP/PS1 mice shows a shift in spine morphology to favour stubby spines ((e), $\chi^2 = 18.15$, $p = 0.03$, Bonferroni's adjusted post hoc test), which was ameliorated by Kv3.4 knockdown both compared to wild-type mice (e) and near and far from plaques (f). Values are reported as the proportion of spines in each category generated from means per mouse.

by 36.3% and 23.2%, respectively, with a bigger effect recorded in WT mice (genotype × treatment interaction $F[1,1102.12]$, $p < 0.0001$). Importantly, Kv3.4 reduction in APP/PS1 mice restored spine density to be not significantly different from WT control level, as confirmed by post hoc estimated marginal means comparisons (Figure 3(a)).

In APP/PS1 mice, dendrites within 30 µm of a plaque edge had lower spine densities than those farther away in both conditions

(Figure 3(b), effect of plaque proximity $F[1,867.22]=172.88$, $p<0.0001$). In comparison to the control condition, Kv3.4 knockdown significantly increased spine densities (effect of treatment, $F[1,867.42]=94.15$, $p<0.0001$) by 32.7% in dendrites far from plaques ($t=-5.78$, $p<0.001$ post hoc comparison) and by 26.4% in dendrites near plaques ($t=-8.59$, $p<0.0001$). This rescue of plaque-associated spine loss with Kv3.4 knockdown is also illustrated when spine density is plotted versus plaque distance (Figure 3(c)).

In addition to spine densities, we also examined dendritic spine morphology, which affects post-synaptic integration of signals. There is a differential distribution of spine shapes in the control hemisphere of APP/PS1 mice with 7× more stubby spines compared to WT control level (Figure 3(e), χ^2 ($p<0.05$) and χ^2 Bonferroni's adjusted post hoc test ($p<0.05$)). Kv3.4 knockdown reduces the number of stubby spines by more than half in these APP/PS1 mice (Figure 3(e)), which is also reflected in Figure 3(f), where dendrites in both hemisphere conditions were further classified according to their plaque proximity. For dendrites distant from plaques and near plaques, the decrease in stubby spines in Kv3.4 knockdown hemisphere relative to control hemisphere appears to be accompanied by a compensatory increase in the proportion of thin spines, but neither of these changes reached significance (Figure 3(f)).

To determine whether the rescue observed in our transgenic mouse line may be relevant to human brain, we examined Kv3.4 in human post-mortem brain samples and human iPSC-derived neuronal cultures. In human iPSC neurons derived from blood samples from five different donors, we observe Kv3.4 in synapses along dendrites (Figure 4), demonstrating the presence of Kv3.4 protein in human synapses. Interestingly, challenging these neurons with human AD brain homogenate containing Aβ causes a decrease in Kv3.4 expression alongside an increase in curvature of MAP2 positive neurites compared to AD brain homogenate immunodepleted to remove Aβ (Figure 5, ANOVA of linear mixed-effects model of data transformed with the formula $(\text{Tortuosity}-1)^{1/7}$ to fit assumptions of model: $F[1,6944]=15.21$, $p<0.0001$). In human brain from people with very low (Braak 0–I), moderate (Braak III–IV) and extensive (Braak V–VI) Alzheimer's disease pathology, we confirm that Kv3.4 is expressed in both frontal and temporal cortices (Brodmann areas 9 and 20/21, respectively). In our samples, we do not observe any difference in levels between Braak stages or brain regions (linear model with Braak stage group, brain region, age, sex and post-mortem interval (PMI) as fixed effects: effect of Braak stage group $F[2,50]=0.092$, $p=0.91$; effect of brain region $F[1,50]=0.626$, $p=0.43$, data Tukey transformed to meet assumptions of linear model). There were also no effects of sex, age or PMI in our analyses (Supplemental Figure 2).

Discussion

The loss of synapses has implications for the impaired learning and memory in Alzheimer's patients considering the strong correlation between synapse loss and cognitive decline in disease (DeKosky et al., 1996; DeKosky and Scheff, 1990; Terry et al., 1991). Further the plasticity of synapses and ability to target synaptic receptors makes them attractive therapeutic targets. Based on previous data showing elevated expression of Kv3.4 around Aβ plaques in human AD brain and in model systems (Angulo et al., 2004; Boscia et al., 2017; Pannaccione et al., 2007), here we tested the hypothesis that Kv3.4 is involved in synapse loss in the APP/PS1 mouse model of amyloidopathy. Previous work using Kv3.4 downregulation, either through siRNA or a selective toxin blocker, has shown neuroprotective effects in hippocampal cultures and in Tg2576 mice (Boscia et al., 2017; Ciccone et al., 2019; Pannaccione et al., 2007). In this study, we observed that the downregulation of Kv3.4 using clustered regularly interspaced short palindromic repeats (CRISPR)/Cas9 AAV ameliorates plaque-associated dendritic spine loss in APP/PS1 mice. Upon examination of cortical pyramidal neurons, we found dendritic spine loss in APP/PS1 mice which is exacerbated near plaques, in agreement with previous findings in several different plaque-bearing transgenic mice (Koffie et al., 2009; Moolman et al., 2004; Rozkalne et al., 2011; Spires, 2005). Kv3.4 knockdown rescues this phenotype in APP/PS1 mice, restoring spine density to WT control levels. Given their ability to impact membrane depolarisation and neurotransmitter release, it certainly anticipated that the fine control of potassium (and indeed other) channel expression at synapses will act as a regulator of synaptic activity in several brain regions. Dendritic spines make up the post-synaptic element of over 90% of cortical excitatory synapses; thus, our findings indicate that Kv3.4 downregulation alleviates synapse loss in plaque-bearing mice. Although we did not replicate published findings (Angulo et al., 2004) showing increased Kv3.4 levels in human AD brain compared to controls, we do observe Kv3.4 specifically localised to synapses in human iPSC-derived cortical neurons, supporting the possibility that Kv3.4 in human synapses may mediate Aβ-induced synaptotoxicity.

One potential mechanism linking Aβ to Kv3.4 is that oligomeric Aβ promotes the generation of Ca^{2+}-induced reactive oxygen species (ROS) and activates the transcriptional factor nuclear factor kappa-B (NF-κB) that in turn upregulates Kv3.4 gene expression. The upregulated expression of Kv3.4 mediates excessive K^+ efflux, leading to the activation of caspase-3 (Piccialli et al., 2020). Caspase-3 has been implicated in spine degeneration and consequent synaptic failure (D'Amelio et al., 2011) as well as to the accumulation of tau in neurofibrillary tangles (De Calignon et al., 2010; Spires-Jones et al., 2008). Caspase-3-activated calcineurin has been shown to drive the internalisation of α-amino-3-hydroxy-5-methyl-4-isoxazolepropionic acid (AMPA) receptors from post-synaptic sites, and this is sufficient to cause spine elimination and the loss of synaptic *N*-methyl-D-aspartate receptor (NMDA) receptors (D'Amelio et al., 2011; Hsieh et al., 2006; Snyder et al., 2005). Our previous work in mouse models has demonstrated that lowering calcineurin levels is also protective against dendritic spine loss in mouse models (Rozkalne et al., 2011; Wu et al., 2010). Elevated ROS production, NF-κB activity and K^+ efflux are also prerequisites for the formation of microglial and astrocytic inflammasomes (Venegas and Heneka Michael, 2019), and data are accumulating linking both microglia and astrocytes to synapse loss in AD models (Henstridge et al., 2019; S. Hong et al., 2016; Litvinchuk et al., 2018). It is also noteworthy that Kv3.4 is expressed in astrocytes in addition to neurones where it is upregulated in models of AD (Boscia et al., 2017). Hence, a direct impact of Kv3.4 downregulation on the reactive astrocytes in the AD brain may also deliver an additional and useful benefit alongside the impact on neuronal synaptic health quantified in details here. Another potential explanation for the spine density recovery observed in our APP/PS1 mice is that

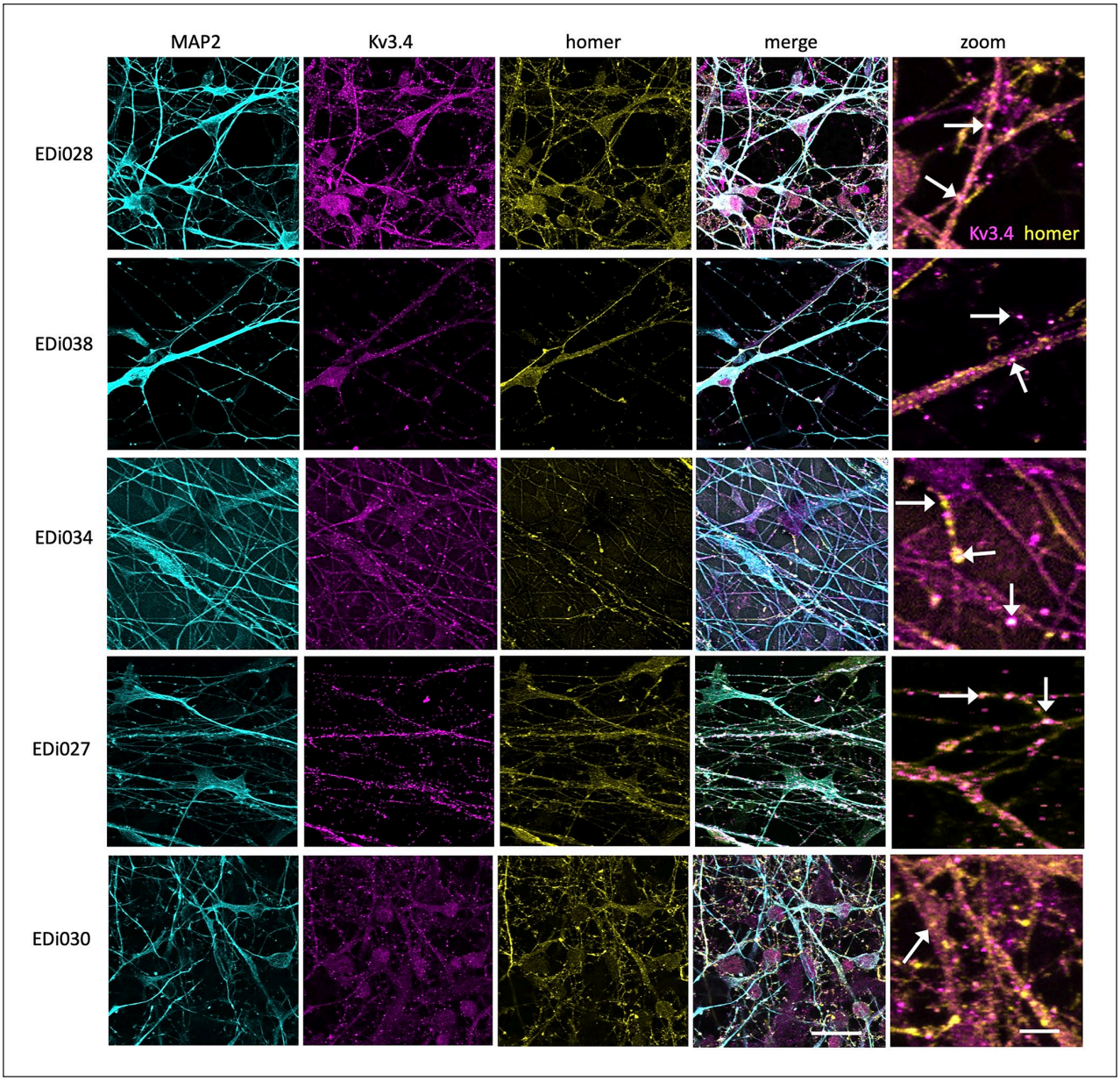

Figure 4. iPSC-derived cortical neurons from five human donors (lines EDi027, EDi028, EDi030, EDi034, EDi038) stained with MAP2 to label dendrites (cyan), post-synaptic protein homer 1 (yellow) and Kv3.4 (magenta) have Kv3.4 positive synaptic puncta along dendrites (arrows in zoom). Scale bar represents 20 µm (5 µm in zoom on right column).

reducing Kv3.4 may have an effect on synapses independent of Aβ. This is supported by our data showing that knockdown of Kv3.4 also increased spine density in WT mice.

In addition to the impact on synapse density, we also observed changes in the proportion of specific spine types, noting a clear increase in the number of stubby spines in APP/PS1 mice. This observation has been reported in numerous studies using cortical biopsies from AD patients, and transgenic mice carrying a familial-AD associated mutant *APP* transgene (Androuin et al., 2018; Spires-Jones et al., 2007; Tackenberg and Brandt, 2009). Studies in hippocampal cultures as well as in vivo in mice further revealed a gradual change from mushroom to stubby spines upon Aβ (Penazzi et al., 2016), highlighting the impact of Aβ on dendritic spine dynamics. While stubby spines are suggested to be the morphological correlate of long-term depression (LTD) induction downstream of Aβ (Li et al., 2009), the loss of mushroom spines is seen as a morphological marker for synaptic failure (Tackenberg and Brandt, 2009). The increase in stubby spines without significant changes in mushroom spines observed that this study has also been documented in a recent hippocampal slice culture study with acute Aβ treatment (Ortiz-Sanz et al., 2020). In contrast to mature mushroom spines that form strong synaptic connections, stubby spines are immature, more dynamic and relatively scarce in the mature brain (Fiala et al., 1998; Harris et al., 1992). Spine outgrowth and maturation are dependent on NMDA and AMPA receptors (Engert and Bonhoeffer, 1999; Matus, 2000). Assuming

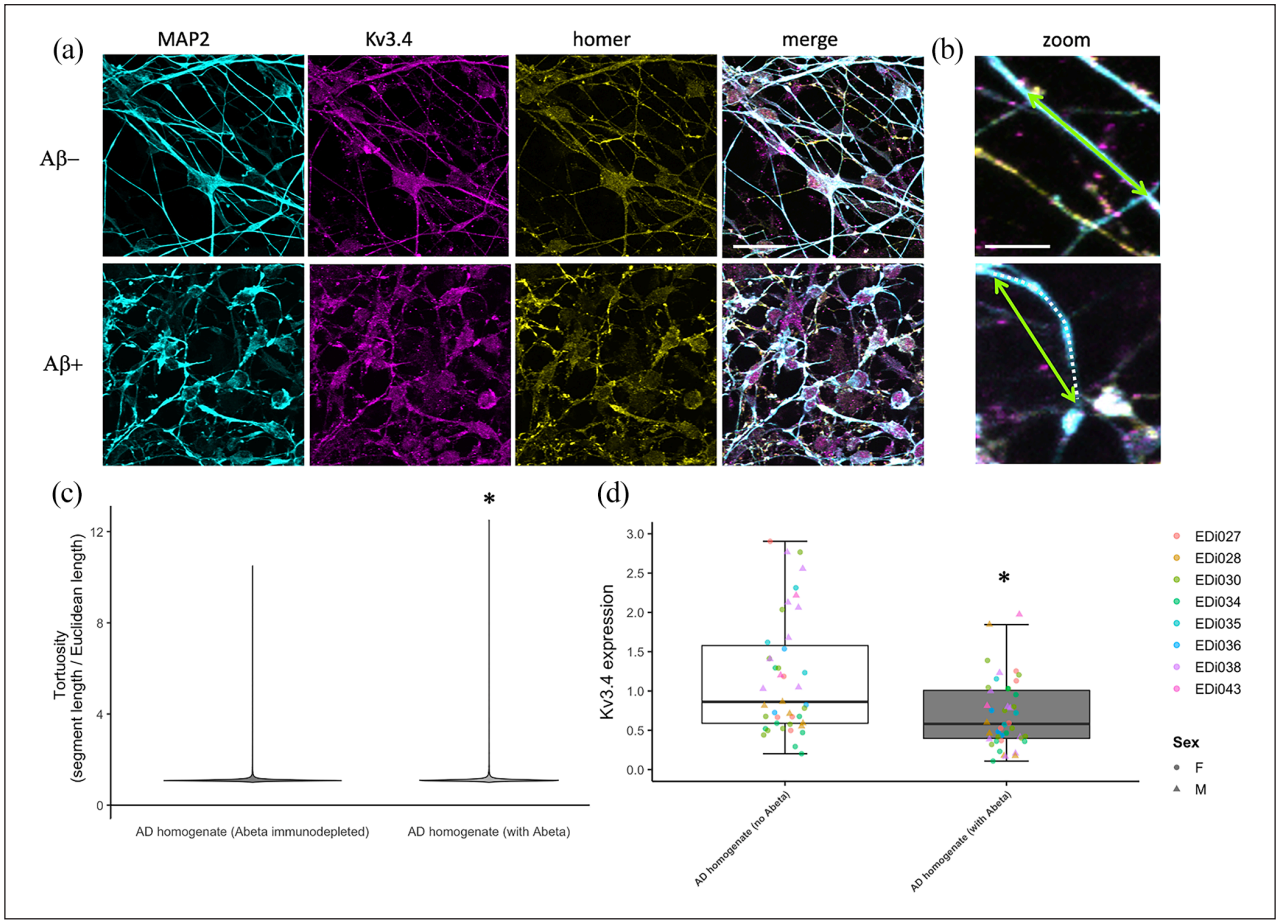

Figure 5. Human iPSC-derived neurons were challenged with homogenate of brain from AD patients either mock immunodepleted for amyloid beta (with Abeta) or immunodepleted to remove Abeta (no Abeta). These neurons were fixed and stained for dendrites (MAP2, cyan) and dendrite tortuosity was measured as the dendritic segment length (magenta dotted line) divided by the direct Euclidean distance between the ends of the segment (green arrows, (a)). A violin plot of tortuosity shows an increase in curvature of dendrites treated with Aβ containing AD brain homogenate ((b), * ANOVA on linear mixed-effects model of transformed data with experiment and image nested in line as a random effect, $F[1,6944]$, $p < 0.0001$). AD brain homogenate also causes a decrease in Kv3.4 expression as measured by qPCR ((c), * ANOVA on linear mixed-effects model with experiment nested in line as a random effect, $F[1,47] = 25.55$, $p < 0.0001$). Scale bars represent 20 µm in (a) and 5 µm in (b).

that the spine loss detected in our APP/PS1 mice was a result of caspase-3-induced AMPA receptor endocytosis, the resulting loss of both AMPA and NMDA receptors may explain the increased number of immature stubby spines in our transgenic mice. Fundamentally, changes in spine morphology affect the post-synaptic integration of signals. While the volume of the spine head is important for the expressions of NMDA and AMPA receptors (Matsuzaki et al., 2001, 2004), the spine neck is responsible for Ca^2+ compartmentalisation (Grunditz et al., 2008). Ca^2+ imaging studies demonstrated a drastic increase in accumulated Ca^2+ at the base of short stubby spines devoid of a neck (Noguchi et al., 2005). This would permit such a copious amount of Ca^2+ to enter the parent dendrite that causes a loss of spine-to-dendrite Ca^2+ homeostasis, as observed through Ca^2+ imaging in APP/PS1 mice (Kuchibhotla et al., 2008). Our observation that Kv3.4 knockdown shifts spine morphology from stubby to thin in APP/PS1 mice is interesting as thin spines become less prevalent alongside age-related cognitive deterioration in monkeys (Dumitriu et al., 2010). Thin spines are thought to be 'learning spines' that are capable of strengthening plasticity in the local circuit (Bourne and Harris, 2007). Thus, the potential of targeting Kv3.4 to increase the proportion of thin spines in AD may also result in restored plasticity and cognitive benefits, as reported in the 17β-estradiol treatment study that targets spine dynamics in rhesus monkeys (Hao et al., 2006).

We observe Kv3.4 protein in dendrites and post-synaptic sites on human neurons derived from five different stem cell donors, which alongside detection of Kv3.4 in human brain tissue confirms this channel is relevant to human brain function. Somewhat counterintuitively, treatment with Aβ containing homogenate lowered expression levels of Kv3.4. We propose that these iPSC-derived neurons are reducing their Kv3.4 expression as a protective mechanism to prevent synaptic toxicity induced by Aβ.

Taken together, our results demonstrate that Kv3.4 downregulation is able to reduce dendritic spine loss and restore spine density and morphology in aged APP/PS1 mice. We also observe Kv3.4 expression on the synapses of human neurons making it a

promising target for the development of novel therapeutic agents that seek to modulate Kv3.4 expression and/or function for the treatment of Alzheimer's disease, and potentially other central nervous system (CNS) diseases.

Declaration of conflicting interests

The author(s) declared the following potential conflicts of interest with respect to the research, authorship and/or publication of this article: T.L.S.J. received funding from Autifony Therapeutics Limited and an anonymous industry partner and is on the Scientific Advisory Board of Cognition Therapeutics.

Funding

The author(s) disclosed receipt of the following financial support for the research, authorship and/or publication of this article: This work was funded by Autifony Therapeutics Limited, Alzheimer's Research UK (ARUK-TVPG2018-010), the UK Dementia Research Institute, which receives its funding from DRI Ltd, funded by the UK Medical Research Council, Alzheimer's Society and Alzheimer's Research UK, and the European Research Council (ERC) under the European Union's Horizon 2020 research and innovation programme under grant agreement no. 681181, NIH grant R56-AG072473 (M.J.M.R.) and the Emory Alzheimer's Disease Research Center grant 00100569 (M.J.M.R.).

ORCID iD

Tara L. Spires-Jones https://orcid.org/0000-0003-2530-0598

Supplemental material

Supplemental material for this article is available online.

References

Androuin A, Potier B, Nägerl UV, et al. (2018) Evidence for altered dendritic spine compartmentalization in Alzheimer's disease and functional effects in a mouse model. *Acta Neuropathologica* 135(6): 839–854.

Angulo E, Noé V, Casadó V, et al. (2004) Up-regulation of the Kv3.4 potassium channel subunit in early stages of Alzheimer's disease. *Journal of Neurochemistry* 91(3): 547–557.

Bakdash JZ and Marusich LR (2017) Repeated measures correlation. *Frontiers in Psychology* 8: 456.

Boscia F, Pannaccione A, Ciccone R, et al. (2017) The expression and activity of KV3.4 channel subunits are precociously upregulated in astrocytes exposed to Aβ oligomers and in astrocytes of Alzheimer's disease Tg2576 mice. *Neurobiology of Aging* 54: 187–198.

Bourne J and Harris KM (2007) Do thin spines learn to be mushroom spines that remember? *Current Opinion in Neurobiology* 17(3): 381–386.

Ciccone R, Piccialli I, Grieco P, et al. (2019) Synthesis and pharmacological evaluation of a novel peptide based on anemonia sulcata BDS-I toxin as a new KV3.4 inhibitor exerting a neuroprotective effect against amyloid-β peptide. *Frontiers in Chemistry* 7: 479.

Colom-Cadena M, Spires-Jones T, Zetterberg H, et al. (2020) The clinical promise of biomarkers of synapse damage or loss in Alzheimer's disease. *Alzheimer's Research & Therapy* 12(1): 21.

D'Amelio M, Cavallucci V, Middei S, et al. (2011) Caspase-3 triggers early synaptic dysfunction in a mouse model of Alzheimer's disease. *Nature Neuroscience* 14(1): 69–76.

De Calignon A, Fox LM, Pitstick R, et al. (2010) Caspase activation precedes and leads to tangles. *Nature* 464(7292): 1201–1204.

DeKosky ST and Scheff SW (1990) Synapse loss in frontal cortex biopsies in Alzheimer's disease: Correlation with cognitive severity. *Annals of Neurology* 27(5): 457–464.

DeKosky ST, Scheff SW and Styren SD (1996) Structural correlates of cognition in dementia: Quantification and assessment of synapse change. *Neurodegeneration: A Journal for Neurodegenerative Disorders, Neuroprotection, and Neuroregeneration* 5(4): 417–421.

Dumitriu D, Hao J, Hara Y, et al. (2010) Selective changes in thin spine density and morphology in monkey prefrontal cortex correlate with aging-related cognitive impairment. *The Journal of Neuroscience: The Official Journal of the Society for Neuroscience* 30(22): 7507–7515.

Engert F and Bonhoeffer T (1999) Dendritic spine changes associated with hippocampal long-term synaptic plasticity. *Nature* 399(6731): 66–70.

Fiala JC, Feinberg M, Popov V, et al. (1998) Synaptogenesis via dendritic filopodia in developing hippocampal area CA1. *Journal of Neuroscience* 18(21): 8900–8911.

Grunditz A, Holbro N, Tian L, et al. (2008) Spine neck plasticity controls postsynaptic calcium signals through electrical compartmentalization. *The Journal of Neuroscience: The Official Journal of the Society for Neuroscience* 28(50): 13457–13466.

Hao J, Rapp PR, Leffler AE, et al. (2006) Estrogen alters spine number and morphology in prefrontal cortex of aged female rhesus monkeys. *The Journal of Neuroscience: The Official Journal of the Society for Neuroscience* 26(9): 2571–2578.

Harris KM, Jensen FE and Tsao B (1992) Three-dimensional structure of dendritic spines and synapses in rat hippocampus (CA1) at postnatal day 15 and adult ages: Implications for the maturation of synaptic physiology and long-term potentiation. *The Journal of Neuroscience: The Official Journal of the Society for Neuroscience* 12(7): 2685–2705.

Henstridge CM, Hyman BT and Spires-Jones TL (2019) Beyond the neuron-cellular interactions early in Alzheimer disease pathogenesis. *Nature Reviews Neuroscience* 20(2): 94–108.

Hong S, Beja-Glasser VF, Nfonoyim BM, et al. (2016) Complement and microglia mediate early synapse loss in Alzheimer mouse models. *Science* 352(6286): 712–716.

Hong W, Wang Z, Liu W, et al. (2018) Diffusible, highly bioactive oligomers represent a critical minority of soluble Aβ in Alzheimer's disease brain HHS public access. *Acta Neuropathologica* 136(1): 19–40.

Hsieh H, Boehm J, Sato C, et al. (2006) AMPAR removal underlies Aβ-induced synaptic depression and dendritic spine loss. *Neuron* 52(5): 831–843.

Jankowsky JL, Fadale DJ, Anderson J, et al. (2004) Mutant presenilins specifically elevate the levels of the 42 residue beta-amyloid peptide in vivo: Evidence for augmentation of a 42-specific gamma secretase. *Human Molecular Genetics* 13(2): 159–170.

Kääb S, Miguel-Velado E, López-López JR, et al. (2005) Down regulation of Kv3.4 channels by chronic hypoxia increases acute oxygen sensitivity in rabbit carotid body: Ion channel remodelling by chronic hypoxia. *The Journal of Physiology* 566(2): 395–408.

Kaczmarek LK and Zhang Y (2017) Kv3 channels: Enablers of rapid firing, neurotransmitter release, and neuronal endurance. *Physiological Reviews* 97(4): 1431–1468.

Koffie RM, Hashimoto T, Tai H-C, et al. (2012) Apolipoprotein E4 effects in Alzheimer's disease are mediated by synaptotoxic oligomeric amyloid-β. *Brain* 135(7): 2155–2168.

Koffie RM, Meyer-Luehmann M, Hashimoto T, et al. (2009) Oligomeric amyloid β associates with postsynaptic densities and correlates with excitatory synapse loss near senile plaques. *Proceedings of the National Academy of Sciences* 106(10): 4012–4017.

Kuchibhotla KV, Goldman ST, Lattarulo CR, et al. (2008) Abeta plaques lead to aberrant regulation of calcium homeostasis in vivo resulting in structural and functional disruption of neuronal networks. *Neuron* 59(2): 214–225.

Li S, Hong S, Shepardson NE, et al. (2009) Soluble oligomers of amyloid β-protein facilitate hippocampal long-term depression by disrupting neuronal glutamate uptake. *Neuron* 62(6): 788–801.

Litvinchuk A, Wan Y-W, Swartzlander DB, et al. (2018) Complement C3aR inactivation attenuates tau pathology and reverses an immune network deregulated in tauopathy models and Alzheimer's disease. *Neuron* 100(6): 1337–1353.e5.

Matsuzaki M, Ellis-Davies GC, Nemoto T, et al. (2001) Dendritic spine geometry is critical for AMPA receptor expression in hippocampal CA1 pyramidal neurons. *Nature Neuroscience* 4(11): 1086–1092.

Matsuzaki M, Honkura N, Ellis-Davies GCR, et al. (2004) Structural basis of long-term potentiation in single dendritic spines. *Nature* 429(6993): 761–766.

Matus A (2000) Actin-based plasticity in dendritic spines. *Science* 290(5492): 754–758.

Moolman DL, Vitolo OV, Vonsattel J-PG, et al. (2004) Dendrite and dendritic spine alterations in Alzheimer models. *Journal of Neurocytology* 33(3): 377–387.

Noguchi J, Matsuzaki M, Ellis-Davies GCR, et al. (2005) Spine-neck geometry determines NMDA receptor-dependent Ca2+ signaling in dendrites. *Neuron* 46(4): 609–622.

Ortiz-Sanz C, Gaminde-Blasco A, Valero J, et al. (2020) Early effects of Aβ oligomers on dendritic spine dynamics and arborization in hippocampal neurons. *Frontiers in Synaptic Neuroscience* 12: 2.

Pannaccione A, Boscia F, Scorziello A, et al. (2007) Up-regulation and increased activity of KV3.4 channels and their accessory subunit MinK-related peptide 2 induced by amyloid peptide are involved in apoptotic neuronal death. *Molecular Pharmacology* 72(3): 665–673.

Penazzi L, Tackenberg C, Ghori A, et al. (2016) Aβ-mediated spine changes in the hippocampus are microtubule-dependent and can be reversed by a subnanomolar concentration of the microtubule-stabilizing agent epothilone D. *Neuropharmacology* 105: 84–95.

Peters A and Kaiserman-Abramof IR (1970) The small pyramidal neuron of the rat cerebral cortex. The perikaryon, dendrites and spines. *American Journal of Anatomy* 127(4): 321–355.

Piccialli I, Ciccone R and Pannaccione A (2020) The new Kv3.4 inhibitor BDS-I[1-8] as a potential pharmacological opportunity in Alzheimer's disease therapy. *Neural Regeneration Research* 15(7): 1255–1256.

Rowan MJM and Christie JM (2017) Rapid state-dependent alteration in Kv3 channel availability drives flexible synaptic signaling dependent on somatic subthreshold depolarization. *Cell Reports* 18(8): 2018–2029.

Rowan MJM, DelCanto G, Yu JJ, et al. (2016) Synapse-level determination of action potential duration by K+ channel clustering in axons. *Neuron* 91(2): 370–383.

Rozkalne A, Hyman BT and Spires-Jones TL (2011) Calcineurin inhibition with FK506 ameliorates dendritic spine density deficits in plaque-bearing Alzheimer model mice. *Neurobiology of Disease* 41(3): 650–654.

Schneider CA, Rasband WS and Eliceiri KW (2012) NIH image to imageJ: 25 years of image analysis. *Nature Methods* 9(7): 671–675.

Serrano-Pozo A, Frosch MP, Masliah E, et al. (2011) Neuropathological alterations in Alzheimer disease. *Cold Spring Harbor Perspectives in Medicine* 1(1): a006189.

Shi Y, Kirwan P and Livesey FJ (2012) Directed differentiation of human pluripotent stem cells to cerebral cortex neurons and neural networks. *Nature Protocols* 7(10): 1836–1846.

Snyder EM, Nong Y, Almeida CG, et al. (2005) Regulation of NMDA receptor trafficking by amyloid-β. *Nature Neuroscience* 8(8): 1051–1058.

Song MS, Ryu PD and Lee SY (2017) Kv3.4 is modulated by HIF-1α to protect SH-SY5Y cells against oxidative stress-induced neural cell death. *Scientific Reports* 7(1): 2075.

Spires TL (2005) Dendritic spine abnormalities in amyloid precursor protein transgenic mice demonstrated by gene transfer and intravital multiphoton microscopy. *Journal of Neuroscience* 25(31): 7278–7287.

Spires-Jones TL and Hyman BT (2014) The intersection of amyloid beta and tau at synapses in Alzheimer's disease. *Neuron* 82(4): 756–771.

Spires-Jones TL, de Calignon A, Matsui T, et al. (2008) In vivo imaging reveals dissociation between caspase activation and acute neuronal death in tangle-bearing neurons. *Journal of Neuroscience* 28(4): 862–867.

Spires-Jones TL, Meyer-Luehmann M, Osetek JD, et al. (2007) Impaired spine stability underlies plaque-related spine loss in an Alzheimer's disease mouse model. *The American Journal of Pathology* 171(4): 1304–1311.

Tackenberg C and Brandt R (2009) Divergent pathways mediate spine alterations and cell death induced by amyloid-beta, wild-type tau, and R406W tau. *The Journal of Neuroscience: The Official Journal of the Society for Neuroscience* 29(46): 14439–14450.

Terry RD, Masliah E, Salmon DP, et al. (1991) Physical basis of cognitive alterations in Alzheimer's disease: Synapse loss is the major correlate of cognitive impairment. *Annals of Neurology* 30(4): 572–580.

Toombs J, Panther L, Ornelas L, et al. (2020) Generation of twenty four induced pluripotent stem cell lines from twenty four members of the Lothian Birth Cohort 1936. *Stem Cell Research* 46: 101851.

Venegas C and Heneka M (2019) Inflammasome-mediated innate immunity in Alzheimer's disease. *FASEB J* 33: 13075–13084.

Wu H-Y, Hudry E, Hashimoto T, et al. (2010) Amyloid induces the morphological neurodegenerative triad of spine loss, dendritic simplification, and neuritic dystrophies through calcineurin activation. *Journal of Neuroscience* 30(7): 2636–2649.

Zhang Y and Kaczmarek LK (2016) Kv3.3 potassium channels and spinocerebellar ataxia. *The Journal of Physiology* 594(16): 4677–4684.